Numerical analysis on temporal size change of expiratory droplets by considering component variation

Yunchen Bu[1*], *Ryozo* Ooka[2], *Hideki* Kikumoto[2], and *Wonseok* Oh[2]
[1]Graduate School of Engineering, The University of Tokyo, 4-6-1 Komaba, Meguro-ku, Tokyo 153-8505, Japan
[2]Institute of Industrial Science, The University of Tokyo, 4-6-1 Komaba, Meguro-ku, Tokyo 153-8505, Japan

Abstract. When conducting computational fluid dynamics (CFD) simulations to investigate the evaporation characteristics of respiratory particles, the over-simplification of droplet compositions may cause inaccuracies in the results. Although some researchers have conducted parametric studies on droplet components, an investigation using CFD simulation is still lacking. Therefore, this study aimed to determine the effect of different components on the temporal size change of expiratory droplets using CFD simulation. Two droplet sizes (10 μm and 100 μm) were selected, and two types of component combinations were considered, both with a volume fraction of 98.2% for water and 1.8% for non-volatile parts. In Scenario 1, the non-volatile part is composed of NaCl (density: 2200 kg/m^3, molecular weight: 58.5 kg/kmol), whereas in Scenario 2, the non-volatile part is composed of NaCl, KCl, lactate, and protein (density: 1000 kg/m^3, average molecular weight: 293 kg/kmol). Computations were conducted under constant temperature (25 °C) and different relative humidity (0 and 90%). The results showed that the equilibrium size and equilibrium time were strongly dependent on the droplet components. In subsequent investigations, the effects of different droplet components should be considered in the CFD simulations to obtain more accurate results.

1 Introduction

In recent years, CFD simulations have been widely used during great pandemics to investigate the evaporation and dispersion of expiratory particles [1–5]. Due to the uncertainty of exact droplet components and for simplification, most CFD studies have assumed the droplet components to be water or saline [1–3]. However, this may have contributed to the inaccuracy of the simulation results. Some studies have investigated the effects of different droplet component assumptions on evaporation behavior. For example, Redrow et al. [4], for the first time, considered different chemical components (pure water, saline solution, and complete sputum) of expiratory droplets; Oliveira et al. [5] also considered the effects of low protein and high protein content. All these studies are based on calculations of theoretical models, facilitating quicker calculations but with less consideration of more complex situations involving air turbulence.

Therefore, to fill in the gaps in the current research, this study conducted an investigation using CFD simulation to enable a more accurate prediction of the effects of different component assumptions on the temporal evaporation behavior of expiratory droplets.

2 Methods

2.1 Mathematic models

In this simulation, the Eulerian method was used to represent the continuous phase—comprising dry air and water vapor. The Lagrangian method was applied to model discrete phases—droplets passing through the evaporation process.

2.1.1 Heat and mass transfer models for a moving pure-water droplet

The diffusive mass change rate of a pure-water particle during the evaporation process can be expressed as shown in equation (1) [6,7]:

$$\frac{\mathrm{d}m_\mathrm{p}}{\mathrm{d}t} = -g^* A_\mathrm{S} \ln(1+B) \tag{1}$$

where m_p is the mass of the particle (kg), g^* is the mass transfer conductance (g/m^2·s), and A_S is the surface area of the particle (m^2). $B = (Y_{\mathrm{v}\infty} - Y_\mathrm{vr})/(Y_\mathrm{vr} - 1)$ is the Spalding transfer number, where $Y_{\mathrm{v}\infty}$ is the vapor mass fraction far away from the particle, and Y_vr is the vapor mass fraction at the particle surface.

The radius change rate of the droplet can be further obtained as follows by deriving equation (1) into equation (2), which was originally developed by Kukkonen et al. [8]:

$$\frac{\mathrm{d}r_\mathrm{p}}{\mathrm{d}t} = -\frac{D_\infty M_\mathrm{v} p_\mathrm{T} \mathrm{Sh}}{\rho_\mathrm{p} r_\mathrm{p} R T_\infty} \ln \frac{(p_\mathrm{T} - p_{\mathrm{v}\infty})}{(p_\mathrm{T} - p_\mathrm{vr})} \tag{2}$$

Here, r_p is the particle radius (m), t is the time (s), D_∞ is the binary diffusivity of water vapor in the air (m^2/s), M_v is the molecular weight of water vapor (kg/kmol), p_T is the total pressure (Pa), ρ_p is the density of the particle (kg/m^3), r_p is the radius of the particle (m), R is the universal gas constant (J/kmol·K), T_∞ is

Corresponding author: bychen@iis.u-tokyo.ac.jp

the ambient air temperature (K), $p_{v\infty}$ is the vapor pressure far away from the particle (Pa), and p_{vr} is the vapor pressure at the particle surface that is assumed to be saturated (Pa). $Sh = 1 + 0.3Re_p^{1/2}Sc^{1/3}$ is the Sherwood number, where Re_p is the droplet Reynolds number, Sc is the Schmidt number; the Sherwood number, which represents the ratio between convective and the diffusive mass transfer, considers the effect of relative velocity between the droplet and the ambient air on the droplet mass transfer [1].

The particle energy balance can be expressed as shown in equation (3) [1,7]:

$$m_p c_p \frac{dT_p}{dt} = Q_t + Q_{rad} + Q_L \quad (3)$$

where c_p is the specific heat capacity of water (J/kg·K), Q_t is the rate of convective heat transfer from the ambient flow to the particle (W), Q_{rad} is the rate of radiative heat transfer (W), Q_L is the rate of latent heat transfer (W).

The temperature change rate of the droplet can be further expressed as shown in Equation (4) [7].

$$\frac{dT_p}{dt} = \frac{3}{\rho_p r_p c_p}[fK_g\frac{T_\infty - T_p}{r_p}Nu + Q_{a,p}(\frac{1}{4}G - \sigma T_p^4) + L_v\rho_p\frac{dr_p}{dt}] \quad (4)$$

Here, T_p is the particle temperature (K), f is the mass transfer correction, K_g is the thermal conductivity of air (W/m·K), σ is the Stefan-Boltzmann constant (W/(m^2·K^4)), $Q_{a,p}$ is the absorption efficiency of the particle, and G is the incident radiative heat flux. $Nu = 1 + 0.3Re_p^{1/2}Pr^{1/3}$ is the Nusselt number, where Pr is the Prandtl number of ambient air, L_v is the effective latent heat of the droplet vaporization (J/kg); the Nusselt number, which represents the ratio between convective and conductive heat transfer, considers the effect of the relative velocity between the droplet and the ambient air on the droplet heat transfer [1].

2.1.2 Modifications for a multi-component droplet

For a multicomponent droplet containing soluble salts, the saturation vapor pressure at the droplet surface is less than that of a pure water droplet because of Raoult's law [1,7]:

$$p_{vr,s} = \chi_w p_{vr}(T_p) \quad (5)$$

Here, $p_{vr,s}$ is the saturation vapor pressure of a droplet containing dissolved solute (Pa), χ_w is the mole fraction of water, which can be calculated using Equation (6) [1]:

$$\chi_w = \frac{n_w}{n_s + n_w} = (1 + \frac{6im_sM_w}{\pi\rho_w M_s d_p^3})^{-1} \quad (6)$$

where n_w is the amount of water in moles (kmol), n_s is the amount of solute in moles (kmol), i is the ion factor (the number of ions that one molecule of a substance dissociates into), m_s is the mass of the solute in the droplet (kg), M_s is the molecular weight of the solute (kg/kmol), M_w is the molecular weight of water (kg/kmol), ρ_w is the density of water (kg/m^3), and d_p is the droplet diameter (m).

2.1.3 Equilibrium size for a multi-component droplet

Considering the modifications in Equation (5), Equation (1) can be transformed into Equation (7) for a multicomponent droplet:

$$\frac{dr_p}{dt} = -\frac{D_v M_v p_T Sh}{\rho_p r_p R T_\infty}\ln\frac{(p_T - p_{v\infty})}{(p_T - p_{vr,s})} \quad (7)$$

From Equation (7), we know that the droplet status depends on the relationship between $p_{v\infty}$ and $p_{vr,s}$. When $p_{vr,s} > p_{v\infty}$, $dr_p/dt < 0$, the droplet will keep evaporating; when $p_{vr,s} = p_{v\infty}$, $dr_p/dt = 0$, the droplet will stop evaporating; when $p_{vr,s} < p_{v\infty}$, $dr_p/dt > 0$, the droplet will condensate.

The Kelvin effect indicates that the saturated vapor pressure at the droplet surface is higher than that at the plane surface, which can be written as follows [9]:

$$\ln\frac{p_{vr}}{p_{sat}} = \frac{2M_w\sigma_{LV}}{\rho_w R T_\infty r_p} \quad (8)$$

Here, p_{sat} is the saturation vapor pressure at a flat surface with the same temperature as the droplet (Pa), and σ_{LV} is the surface tension of the liquid/vapor interface (J^2/m).

Due to the Kelvin effect, for a pure water droplet, $p_{vr} > p_{sat}$, the smaller r_p becomes, the larger p_{vr}/p_{sat} will be. Moreover, due to the higher temperature of the droplet in an ambient environment, $p_{sat} > p_{v\infty}$. Therefore, $p_{vr} > p_{v\infty}$, and $dr_p/dt < 0$ will remain negative until all the water evaporates and the droplet evaporates completely.

However, for a multi-component droplet, although $p_{v\infty} < p_{vr}$, due to Raoult's law, $p_{vr,s} < p_{vr}$. Therefore, the relationship between $p_{vr,s}$ and $p_{v\infty}$ depends on $p_{v\infty}$ or the ambient RH. When RH is sufficiently high, $p_{vr,s}$ may reduce to $p_{v\infty}$ at some point. Under these circumstances, the droplet stops evaporating, although some water remains with the non-volatile part. When no disturbance occurs, the droplet size no longer changes and is defined as the equilibrium size in this study.

2.2 Calculation conditions

The computational domain is a chamber with the size of 3.6 m × 2.7 m × 2.5 m (L × W × H), as illustrated in Fig. 1. Droplets were injected into the chamber from a 1-cm-radius nozzle 2 m above the ground. The opposite wall of the nozzle, which is marked as blue, was set as the ventilation exhaust.

The transient simulation was conducted using the commercial CFD code, STAR-CCM+ (Ver. 16.06). Reynolds-averaged Navier–Stokes (RANS) equations with a realizable k-epsilon two-layer model were used for turbulence modeling [7,10]; the SIMPLE method was used for pressure-velocity coupling. The convection terms were discretized using a second-order upwind scheme, and the diffusion terms were discretized using a second-order central scheme. The trimmed cell and prism layers were used for mesh division. The total number of spatial grids is approximately 92,300.

At the present stage, for a better comparison, the initial conditions of the injected particles and environment are set similar to a series of past studies [2,3,11]. As shown in Table 1, the airflow was injected from the nozzle with a temperature of 34 °C and RH of 100%, and the velocity variation over time was shown in Fig. 2. Two droplet sizes (10 μm and 100 μm) were selected—both released in the number of around 10,000 at a temperature of 34 °C and the initial velocities of 10 m/s. The injection time point of the droplets is shown in Fig. 2. The indoor air is stagnant. Computations were conducted under a constant ambient temperature of 25 °C and different relative humidity (RH) of 0 and 90%.

Table 2 lists two typical assumptions of the main droplet compositions adopted in the existing literature, both with a volume fraction of 98.2% for water and 1.8% for non-volatile parts [2,3,11]. In Scenario 1, the non-volatile part is composed of Na^+ and Cl^- (density: 2200 kg/m^3, molecular weight: 58.5 kg/kmol) [12]. In Scenario 2, the nonvolatile part is composed of Na^+, K^+, Cl^-, lactate, and glycoproteins. The density of the mixture is assumed to be 1000 kg/m^3, same as that of water. The average molecular weight of the mixture was calculated to be 293 kg/kmol with an estimation that the glycoprotein molecular weight is 29000 kg/kmol [12,13]. The properties of major mucus species are shown in Table 3.

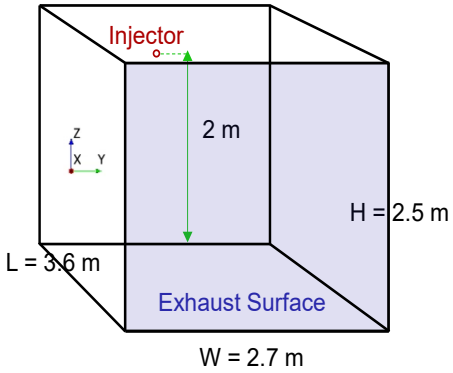

Fig. 1. Geometry and computational domain

Table 1. Boundary conditions

Ventilation exhaust		Pressure outlet
Wall		No slip, Heat insulation
Injector	Flow	T = 34 °C, RH = 100%, Velocity: As shown in Fig. 2
	Droplet	Size: 10 μm, 100 μm T = 34 °C, Velocity: 10 m/s Particle flow rate: Around 10000 particles exhaled simultaneously Direction: Stream-wise

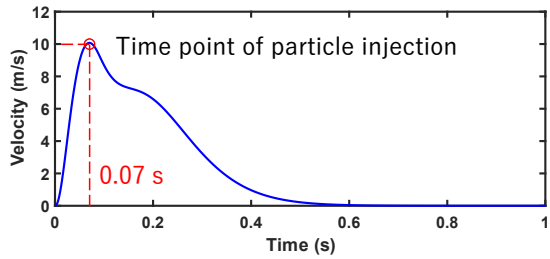

Fig. 2. Velocity variation of injection flow

Table 2. Case settings with different components

Scenario	Non-volatile component	Density (kg/m^3)	Molecular weight (kg/kmol)
1	Na^+, Cl^+	2200	58.5
2	Na^+, K^+, Cl^-, Lactate, Glycoprotein	1000	293

Table 3. Major mucus components for Scenario 2 [12,13]

Species	Molecular weight (kg/kmol)	Concentration (mmol/L)
Na+	23	91 ± 8
K+	39.1	60 ± 11
Cl-	35.5	102 ± 17
Lactate	89	44 ±17
Glycoprotein	29000	76 ±18 (g/L)

3 Results and discussion

Fig. 3 illustrates the simulation results for the spatial distribution of droplets under RH of 90% at 5 s. Two critical characteristics in this study are the "normalized equilibrium size" (the equilibrium size of the droplet over the initial size) and "equilibrium time" (the time required for droplets to reach equilibrium sizes). As shown in Fig. 4 and 5, the shape of the rate of change in droplet size matches well with previous studies using similar settings of computational conditions [2,3,11]. However, because the exact droplet compositions cannot be found in previous papers, there are some distinctions between the plots of the temporal change in droplet size obtained in this CFD calculation and the results achieved by past studies.

As can be seen in Fig. 4, Fig. 5, Table 4 and Table 5, for both 10-μm and 100-μm droplets, in Scenario 1, the normalized equilibrium size is 0.26 at RH = 0% and 0.50 at RH = 90%; in Scenario 2, the normalized equilibrium size is 0.26 at RH = 0% and 0.30 at RH = 90%. From the results, a simple calculation can show that at RH = 0%, the water in the droplet eventually evaporated completely, leaving only the non-volatile portion. We can also see that the droplets did not evaporate completely at an RH of 90% by reaching an equilibrium size at some point in time. Furthermore, the results show that the equilibrium diameters of droplets can be less affected by RH if solutes other than NaCl are considered, possibly because the higher average molecular weight of the non-volatile parts in Scenario 2 increases the surface vapor pressure of a multi-component droplet, making its evaporation performance closer to that of a pure water droplet.

When changing from Scenario 1 to Scenario 2, at RH = 90%, the equilibrium time decreases from 1.43 s to 1.10 s for 10-μm droplets and from 45.3 s to 31.5 s for the 100-μm droplets; at RH = 0%, the equilibrium time decreases from 0.11 s to 0.095 s for the 10-μm droplets and from 3.02 s to 2.63 s for the 100-μm droplets. The results show that the equilibrium time was shorter for Scenario 2. Moreover, we also observed that the time reduction for larger droplets can be more affected by the variation in droplet components, especially at higher relative humidity.

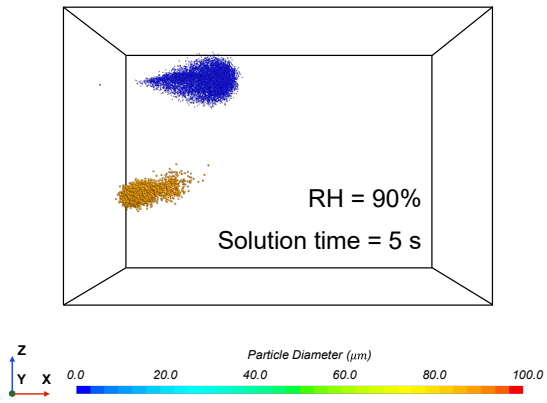

Fig. 3. Illustration of simulation results for spatial distribution of droplets

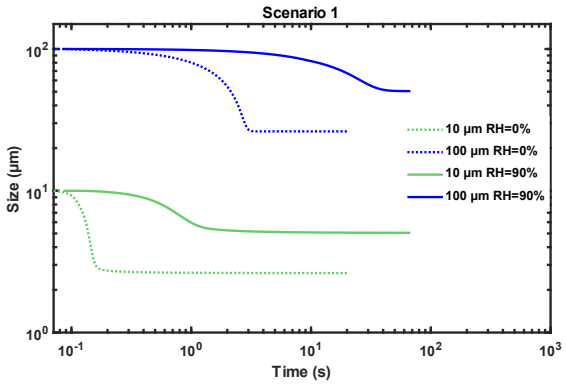

Fig. 4. Plot of the temporal size change for Scenario 1

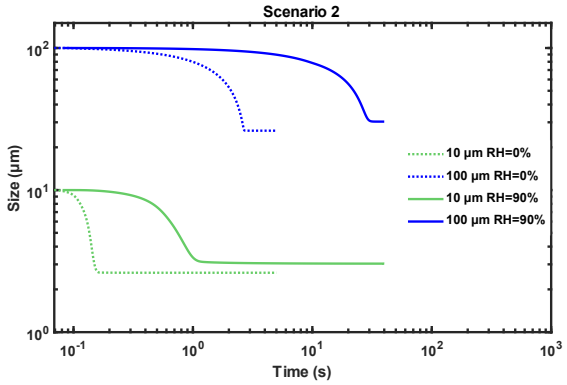

Fig. 5. Plot of the temporal size change for Scenario 2

Table 4. Normalized equilibrium size and time in Scenario 1

Relative humidity	Initial droplet diameter (μm)	Normalized equilibrium size	Equilibrium time (s)
0	10	0.26	0.11
	100	0.26	3.02
90%	10	0.50	1.43
	100	0.50	45.3

Table 5. Normalized equilibrium size and time in Scenario 2

Relative humidity	Initial droplet diameter (μm)	Normalized equilibrium size	Equilibrium time (s)
0	10	0.26	0.095
	100	0.26	2.63
90%	10	0.30	1.10
	100	0.30	31.5

4 Conclusion

In this study, we performed a CFD simulation to investigate the temporal size change of expiratory droplets owing to evaporation and how different component assumptions of droplets affect their equilibrium size and equilibrium time.

In conclusion, the equilibrium size and equilibrium time are strongly dependent on the components of the droplets. In this study, the equilibrium size of droplets in Scenario 2, where the non-volatile parts have lower density and higher average molecular weight, is less affected by the ambient relative humidity; the equilibrium times of different droplet sizes under different relative humidity for Scenario 2 are all shorter than that for Scenario 1. The effects of different droplet components should be considered in subsequent CFD simulations to obtain more accurate results.

References

1. X. Xie, Y. Li, A.T.Y. Chwang, P.L. Ho, W.H. Seto, *How far droplets can move in indoor environments - revisiting the Wells evaporation-falling curve*, Indoor Air. **17** (2007) 211–225.
2. J. Wei, Y. Li, *Enhanced spread of expiratory droplets by turbulence in a cough jet*, Build. Environ. **93** (2015) 86–96.
3. X. Li, Y. Shang, Y. Yan, L. Yang, J. Tu, *Modelling of evaporation of cough droplets in inhomogeneous humidity fields using the multi-component Eulerian-Lagrangian approach*, Build. Environ. **128** (2018) 68–76.
4. J. Redrow, S. Mao, I. Celik, J.A. Posada, Z. gang Feng, *Modeling the evaporation and dispersion of airborne sputum droplets expelled from a human cough*, Build. Environ. **46** (2011) 2042–2051.
5. P.M. De Oliveira, L.C.C. Mesquita, S. Gkantonas, A. Giusti, E. Mastorakos, *Evolution of spray and aerosol from respiratory releases: Theoretical estimates for insight on viral transmission*, Proc. R. Soc. A Math. Phys. Eng. Sci. **477** (2021).
6. D.B. Spalding, *A standard formulation of the steady convective mass transfer problem*, Int. J. Heat Mass Transf. **1** (1960) 192–207.
7. *Particle Heat and Mass Transfer*, Simcenter STAR-CCM+ - User Guid. (2019) 2481.
8. J. Kukkonen, T. Vesala, M. Kulmala, *The interdependence of evaporation and settling for airborne freely falling droplets*, J. Aerosol Sci. **20** (1989) 749–763.
9. L. Liu, J. Wei, Y. Li, A. Ooi, *Evaporation and dispersion of respiratory droplets from coughing*, Indoor Air. **27** (2017) 179–190.
10. Z.J. Zhai, Z. Zhang, W. Zhang, Q.Y. Chen, *Evaluation of various turbulence models in predicting airflow and turbulence in enclosed environments by cfd: Part 1—summary of prevalent turbulence models*, HVAC R Res. **13** (2007) 853–870.
11. Y. Yan, X. Li, J. Tu, *Thermal effect of human body on cough droplets evaporation and dispersion in an enclosed space*, Build. Environ. **148** (2019) 96–106.
12. M. Nicas, W.W. Nazaroff, A. Hubbard, *Toward understanding the risk of secondary airborne infection: Emission of respirable pathogens*, J. Occup. Environ. Hyg. **2** (2005) 143–154.
13. S.P. Grefrath, J.A. Reynolds, *The Molecular Weight of the Major Glycoprotein from the Human Erythrocyte Membrane*, Proc. Natl. Acad. Sci. **71** (1974) 3913–3916.